Water in zeolites of natrolite group and its OH-stretching region in Raman spectroscopy

Water in zeolites of natrolite group and its OH-stretching region in Raman spectroscopy

Amelia Carolina Sparavigna

Department of Applied Science and Technology, Polytechnic University of Turin, Italy

Abstract: Natrolite, $Na_2(Si_3Al_2)O_{10}\cdot 2H_2O$, is a member of a group of zeolite minerals, made of hydrated aluminosilicate minerals. Due to their structure, zeolites have channels, through which water and ions can move. In the RRUFF database, we find the following members of the group: natrolite, mesolite, scolecite, and gonnardite. In the database, Raman spectra are provided where we can easily observe the OH-stretching region of water. We propose the deconvolutions in q-Gaussian functions of these spectra, comparing the obtained results with those available from literature. A review of literature about natrolite is also proposed.

Keywords: Natrolite group minerals, Natrolite, Mesolite, Scolecite, Gonnardite, Raman spectroscopy, q-Gaussian functions, Tsallis statistics, Hydroxyl-stretching Raman region, OH-stretching Raman region, Water ferroelectricity, Thomsonite, Edingtonite.

Introduction

Natrolite, $Na_2(Si_3Al_2)O_{10}\cdot 2H_2O$, is a mineral that was named by M. H. Klaproth, 1803, from Greek 'natron', for its sodium content and 'lithos', that is 'stone' (Strekeisen, 2020). Natrolite is the representative member of a group of zeolites, where zeolites "are hydrated aluminosilicate minerals made from interlinked tetrahedra of alumina (AlO_4) and silica (SiO_4)" (Strekeisen, 2020). The origin of the name 'zeolite', as reported by Strekeisen, is very interesting too. It is told that the term zeolite was proposed by A. F. Cronstedt in 1756, since he "observed that upon rapidly heating the material stilbite, it produced large amounts of steam" (Strekeisen, 2020). Therefore, Cronstedt used Greek 'zeo', to boil, and 'lithos'. Due to their structure, zeolites have channels, through which water and "large ions (such as sodium, potassium, and magnesium)" can "travel into and out of the crystal structure" (Strekeisen, 2020); the size of molecules or ions is controlled by size of channels, and zeolites "can act as a chemical sieve. The term molecular sieve refers to a particular property of these materials: the ability to selectively sort molecules based primarily on a size exclusion process. This is due to a very regular pore structure of molecular dimensions" (Strekeisen, 2020).

In RRUFF database, we find the members of the natrolite group as natrolite, mesolite, scolecite, and gonnardite. In this database, Raman spectra are provided, where we can easily observe the OH-stretching region of water. As we recently made for vivianite and its group, here we propose the deconvolutions in q-Gaussian functions of these spectra, comparing the obtained results with those available from literature. Before the analysis of the Raman spectra, let us propose some properties of natrolite and related literature.

The mineral and its structure

For a general overview of natrolite, let us refer to the Gem Rock web site, a site specific to collectors of minerals. “Is natrolite rare? As a mineral, it’s common”. Let us add that natrolite is present on Mars too; the mineral has been detected by means of the Perseverance rover data (Sarkar et al., 2024). “In terms of properties, natrolite is both pyroelectric and piezoelectric”. “Industrially, what is natrolite used for? As a zeolite mineral, natrolite can be used for ion exchange, gas separation, and catalysis. In fact, natrolite was one of the first zeolites used for ion exchange (meaning magnesium, potassium, sodium, and calcium replace one another when dissolved)” (Gem Rock). “As such, natrolite can be used in chemical filters, water & air purifiers, water softeners, detergents, pet litter, animal feed, wastewater treatment, molecular sieves, soil conditioners”. “Natrolite and mesolite are orthorhombic, while scolecite is monoclinic” (Gem Rock).

Let us consider what the Gem Rock web site is telling about natrolite with more detail, regarding properties and applications. First, we propose the structure of natrolite as given by Paczwa et al., 2016. In the introduction of their article, Paczwa and coworkers stress that the “physical properties of materials entrapped in nano-sized cavities [are] of significant interest for both fundamental science and application of nano-porous compounds. The mineral natrolite is a typical porous compound (zeolite) with the narrow nano-channels”. As previously told, natrolite is orthorhombic, space group Fdd2, with formula units $Na_2Al_2Si_3O_{10}\cdot 2H_2O$. In its framework we find “tetrahedra of alumina (AlO_4) and silica (SiO_4) *chain*s linked together via common *oxygen* atoms”. “The natrolite structure contains channels running parallel to the c-axis and channels connected among themselves by oxygen windows. These oxygen rings create a system of channels, which are placed perpendicular to c-axes” (Paczwa et al., 2016). “The water molecules and sodium ions form zigzag chains along the channel parallel to c-axis. Water molecules occupy two sites in the channels and the other sites are occupied by sodium ions. Each water molecule is coordinated by two framework oxygen atoms and by two sodium ions” (Paczwa et al., 2016).

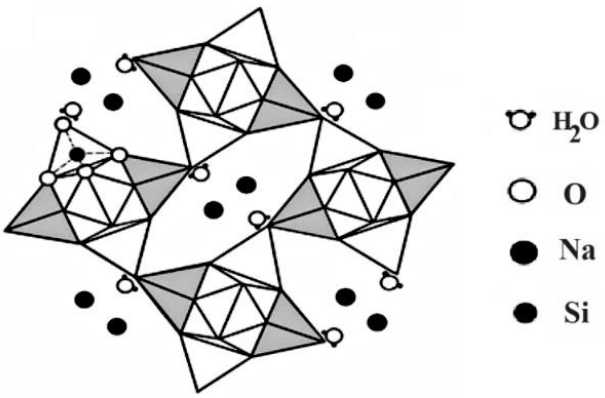

Fig.1 - Natrolite structure projected on the (001) plane, adapted from the Fig.1 by Paczwa et al., 2016 (article distributed under the terms of the Creative Commons Attribution 4.0 International License). The plane of the figure is given as a,b plane. The c-axis is perpendicular to the figure. Natrolite is an orthorhombic crystal. The orthorhombic crystal is obtained by stretching a cubic one, obtaining a rectangular prism, with a rectangular base (a by b) and height (c). The three lattice vectors are mutually orthogonal.

“One of the main features of natrolite is a narrow diameter of channels. The diameter of the oxygen’s windows in the [110] direction is 2.60 A, but the diameter of channel paralleled to the c-axis is only 2.08 A, and it is less than 2.8 A, which is usually assumed for the diameter of water molecule” (Paczwa et al., 2016, Meier, 1960). “Therefore, the interesting problem is the determination of the microscopic mechanism of water molecules mobility in the natrolite channels. The mobility of the water molecules in natrolite was studied … [see references in Paczwa and coworkers]. … the main

kind of mobility of water molecules at high temperature in natrolite is the diffusion along channels parallel to c-axis and water molecule jumps without breaking of one chemical bond of water molecule with sodium ion". Paczwa and coworkers explain that water molecule motion is a "hopping" motion: "the water molecules spend most of their time in a potential well corresponding to equilibrium positions, and only a very small fraction moves between these potential wells" (Paczwa et al., 2016).

Interactions in zeolites

Line and Kearley, 1998, started their discussion about the librational and vibrational spectra of water in natrolite, from the structure of the zeolites. These minerals have "three components: the aluminosilicate framework, …, the extraframework cations or anions which balance the charge of the framework, and the water". The "framework charge is delocalised over the whole framework so that in the first approximation it can either be ignored or regarded as a uniform charge density". "The extraframework cations, on the other hand, are almost fully charged and thus constitute the main bonding centres for any polar species, including water". However, the oxygen sites of the framework make hydrogen bonding to the "hydrogen atoms of the polar species, and it is the strength of this bonding which is often of interest. The water can therefore bind to the cations and/or hydrogen bond to the framework". In the case that we have water–water interactions, "the hydrogen bonding to other water molecules is much stronger than that to the framework and therefore dominates". But in natrolite zeolite, "the water molecules are not directly attached to other water molecules. Thus, the nearest-neighbor interaction from the cation can be studied in isolation". The water molecule is "attached to only two cations and has no water molecules in the first hydration shell" (see please the further discussion of interactions in Line and Kearley, 1998).

"The internal modes of the water molecule are the symmetric (w_1) and asymmetric (w_3) stretch of the OH bonds, and the HOH bend (w_2). The translational modes of the water–sodium cluster are in analogy with the internal modes: one asymmetric Na–O stretch, one symmetric stretch and one mode which changes the Na–O–Na angle. This third mode does not involve significant movement of the water and, in the case of the whole zeolite, the sodium atoms are bound to the aluminosilicate framework" (Line & Kearley, 1998).

Pyroelectricity, piezoelectricity and water ferroelectricity

Returning to the properties of natrolite mentioned by Gem Rock, let us consider pyroelectricity and piezoelectricity. "The experiments, made by Mr. C. A. Meek in the Department of Physics of the University of Manchester … showed conclusively that natrolite is weakly pyroelectric, with a single polar axis, the c-axis. … Since this work was completed, F. Halla and E. Mehl (1932) have found that natrolite is piezoelectric; they do not, however, state which is the piezoelectric axis" (Hey, 1932). Galitskii and Kozlov, 1988, "investigated single natrolite crystals from the Khibinsk and Lovozersk alkaline massifs of the Kola peninsula. The pyroelectric coefficient γ was measured by the static method using temperature steps of 2-3 K … The dielectric constant ε and the tangent of the angle of dielectric losses were determined". Based on the values of γ and ε and comparing with known values for other materials, Galitskii and Kozlov determined the natrolite as a weak linear pyroelectric.

In search for references about piezoelectricity of natrolite, we found mentioned the "water ferroelectricity". Dudka and coworkers, 2020, propose a study to obtain crystal structure refinement of natrolite, for what is regarding the localization of free water. "Traditionally, nanoinclusions (atoms

or molecules) in minerals with pores and channels have been of interest for geologists. … Recently, researchers have been interested in these objects from the fundamental point of view, because inclusions may interact in a special way. In particular, the systems with inclusions in the form of *polar water molecules* have attracted attention. In the absence of chemical interaction, shortrange mutual ordering of the dipole moments of water molecules may occur because of the long-range electric dipole forces. This phenomenon may manifest itself in various (both inorganic and biological) systems. The ordered state of water molecules in a beryl crystal was revealed recently using spectroscopic analysis" (Dudka et al., 2020, mentioning Gorshunov et al., 2016). In general, "information about the characteristics of hydrogen atoms is important for studying the energy of atomic interactions in technological, biological, and pharmaceutical materials. … The most important problem of materials science is the development of hydrogen-storage devices, which may help in solving many climatic and ecological problems" (Dudka et al., 2020). Concluding their work, Dudka and coworkers tell that "XRD analysis of water-containing mineral *natrolite, which is a promising candidate for studying the water ferroelectricity* by spectroscopic methods, was carried out [by them]. … The crystallo-chemical analysis revealed signs of weakness of the bonds of water molecules with the framework. … The obtained data on the orientation of water molecules, their motif, and degree of freedom of their vibrations made it possible to conclude that natrolite is a convenient object for studying the water ferroelectricity by spectroscopic methods" (Dudka et al., 2020).

Ion exchange

Dyer, 2000, explains that the "first scientific allusion to ion exchange is attributed to two English agricultural chemists in 1850. These were J. T. Way and H. S. Thompson, who independently observed the replacement of calcium in soils by ammonium ions. This discovery was the precursor to the study of inorganic materials capable of 'base' exchange, and in 1858 C. H. Eichorn showed that natural zeolite minerals (chabazite and natrolite) could reversibly exchange cations. The importance of this property in water softening was recognized by H. Gans who, at the turn of the century, patented a series of synthetic amorphous aluminosilicates for this purpose". "A broad definition of ion exchange is that it is the transfer of ions across a boundary; this would then cover movement of ions from one liquid phase to another" (Dyer, 2000). "An ideal ion exchange medium is one that fulfils the following criteria: 1. a regular and reproducible composition and structure; 2. high exchange capacity; 3. a rapid rate of exchange (i.e. an open porous structure); 4. chemical and thermal stability and resistance to 'poisoning' as well as radiation stability when used in the nuclear industry; 5. mechanical strength stability and attrition resistance; 6. consistency in particle size, and compatibility with the demands of the use of large columns in industry" (Dyer, 2000). Moreover, in the case of specific applications, it is relevant "the ability to exchange a specific ion(s) *selectively from high concentrations of other ions*. This is particularly true for aqueous *nuclear waste treatment* and in hydrometallurgy" (Dyer, 2000).

Sardashti et al., 2001, studied the "ion-exchange behavior of a natural zeolite from the Zahedan region of Iran toward various heavy-metal cations. The distribution coefficients, equilibrium constant, and Gibbs free energy are calculated from the isotherms data at 298K and 323K as the thermodynamic parameters. ... The ion-exchange experiments of the zeolite are performed to investigate its ability for removing the considered cations from industrial wastewater streams".

Lee et al., 2010, note that, "since its first discovery in nature, natrolite has been largely known as a sodium aluminosilicate zeolite, showing very limited preference toward cation exchange". In their article, Lee and coworkers show that "fully K-exchanged natrolite can be prepared from natural Na-

natrolite under mild aqueous conditions and used to subsequently produce Rb- and Cs-exchanged natrolites. These cation-exchanged natrolites exhibit successive volume expansions by ca. 10, 15.7, and 18.5% for K-, Rb-, and Cs-forms, respectively, compared to the original Na-natrolite". The volume expansion "occurs by converting the elliptical channels into progressively circular ones. The observed cation-dependent changes in the channel volume and shape thus show the flexibility limits of the natrolite framework and suggest the possible existence of compositionally altered analogues in suitable environments as well as a novel means to tailor the cation selectivity of this class of small pore zeolites toward various industrial and environmental applications" (Lee et al., 2010).

"The simultaneous application of high pressure and high temperature has been used to achieve direct ion *exchange of large cesium cations for the small sodium cations* found in the zeolite natrolite by putting it into a *superhydrated* state *with increased pore size.* The larger cations remain trapped upon pressure release, and thus, this method is a means of producing new cationic forms of zeolites" (Hill et al., 2011).

Super-hydrated alkali-metal-exchanged natrolite

Regarding the water in channels, the graphical abstract by Seoung et al., 2013, shows that the "super-hydrated zeolite, $K_{16}Al_{16}Si_{24}O_{80}{\cdot}32\ H_2O$, undergoes a unique transformation above 2.5 GPa whereby the *potassium ions interchange their locations with those of water*, whereas the elliptical channel reverts its major–minor axes, resembling a "chatterbox motion" (see graphics). Alkali-metal-exchanged natrolites under pressure reveal structural changes that far exceed what can be achieved by varying temperature and chemical composition" [for the chatterbox motion, see please video about origami, for instance this one].

Seoung and coworkers prepared a "series of alkali-metal-exchanged natrolites, $A_{16}Al_{16}Si_{24}O_{80}{\cdot}n\ H_2O$ (A=Li, K, Na, Rb, and Cs and n=14, 16, 22, 24, 32)", so that to reveal by means of X-ray diffraction "structural changes that far exceed what can be achieved by varying temperature and chemical composition. The degree of volume expansion caused by *pressure-induced hydration* (PIH) is inversely proportional to the non-framework cation radius". That is, "the expansion of the unit-cell volume through PIH is as large as 20.6 % in Li-natrolite at 1.0 GPa and decreases to 6.7, 3.8, and 0.3 % in Na-, K-, and Rb-natrolites, respectively. On the other hand, the onset pressure of PIH appears to increase with non-framework cation radius up to 2.0 GPa in Rb-natrolite. In Cs-natrolite, no PIH is observed but a new phase forms at 0.3 GPa with a 4.8 % contracted unit cell and different cation–water configuration in the pores" (Seoung et al., 2013). As shown in the graphical abstract, "In K-natrolite, the elliptical channel undergoes a unique *overturn* upon the formation of super-hydrated natrolite $K_{16}Al_{16}Si_{24}O_{80}{\cdot}32\ H_2O$ at 1.0 GPa, a species that reverts back above 2.5 GPa as the potassium ions interchange their locations with those of water and migrate from the hinge to the center of the pores". According to this research, the "Super-hydrated zeolites are new materials that offer numerous opportunities to expand and modify known chemical and physical properties by reversibly changing the composition and structure using pressure in the presence of water" (Seoung et al., 2013).

Neutron diffraction was previously used by Seryotkin and coworkers, 2005, to study "the deuterated natrolite, $Na_{1.85}Mg_{0.05}Ca_{0.03}[Al_{2.06}Si_{2.95}O_{10}]{\cdot}nD_2O$, compressed in liquid D_2O at 0.9 and 1.0 GPa". "At 0.9 GPa, the crystal structure is close to the original natrolite with the same space group Fdd2 and 1% smaller unit cell volume. *New water positions are found in addition to the original ones indicating the early stage of natrolite over-hydration*. The unit cell volume of high-pressure phase stable at 1.0

GPa is expanded by 5.4 % with respect to initial natrolite. According to structural investigations, HP phase contains 3.5 water molecules pfu. Higher degree of hydration is accompanied by the drastic rearrangement of extra-framework subsystem, water molecules occupying four independent positions" (Seryotkin et al., 2005).

Raman spectra of zeolite A framework

In Dutta and Del Barco, 1985, we can find Raman spectroscopic studies of zeolite framework. "Raman spectra of hydrated *zeolite A* completely exchanged with Li^+, Na^+, K^+, Tl^+, and NH_4^+ ions are reported in this paper. The emphasis has been on the high-frequency region between 300 and 1200 cm^{-1}, where the intramolecular modes of the aluminosilicate framework are expected. … In NH_4-A, there is strong spectroscopic evidence for H-bond formation between the cation and the lattice oxygens". What is zeolite A? "Zeolite A, also known as LTA (Linde Type A), belongs to the family of aluminosilicate molecular sieves. It is characterized by the formula $|(Na^+_{12}(H_2O)_{27}|_8[Al_{12}Si_{12}O_{48}]8$ which corresponds to its most common hydrated sodium form (International Zeolite Association - IZA)" (Julbe & Drobek, 2016). Zeolite A is a synthetic zeolite (for a discussion of natural and synthetic materials, see Clifton, 1987). In the Zeolite A, we have Na, Al, Si, O and H as in natrolite. Dutta and Del Barco do not consider the OH-stretching region of Raman spectra.

Natrolite and gases

Ackley and coworkers, 2003, proposed a review regarding the "Application of natural zeolites in the purification and separation of gases". "Patents and other literature have been surveyed to identify the bulk separation and purification processes for which" zeolites have potentialities. The results of the Ackley and coworkers' study is that "natural zeolites are particularly well suited for trace-gas removal. In contrast, they are less likely to provide competitive performance in bulk separations. Clinoptilolite and chabazite are judged the most versatile, while also offering unique adsorption characteristics. Effective and efficient methods for screening all types of adsorbents are presented for various gas separations. … The importance of including relevant process considerations in the analyses is demonstrated through application to processes for a bulk separation (O_2 production from air) and purification (removal of trace levels of N_2O from air). The results are not encouraging for the use of natural zeolites in air separation. Conversely, clinoptilolite and chabazite outperform commercially available synthetics in N_2O removal from air" (Ackley et al., 2003).

Lee and coworkers, 2011, proposed the "pressure-and heat-induced insertion of CO_2 into an auxetic small-pore zeolite". "When the small-pore zeolite natrolite is compressed at ca. 1.5 GPa and heated to ca. 110 °C in the presence of CO_2, the unit cell volume of natrolite expands by 6.8% and ca. 12 wt % of CO_2 is contained in the expanded elliptical channels. This CO_2 insertion into natrolite is found to be reversible upon pressure release" (Lee et al., 2011).

Catalysis

There is a large literature about natrolite and catalysis. Here a few references.

Habibi et al., 2013, proposed a "green synthesis of formamides using the Natrolite zeolite as a natural, efficient and recyclable catalyst". "Chemoselective N-formylation of different amines was carried out with formic acid in the presence of the Natrolite zeolite as an efficient, stable and natural

heterogeneous catalyst to give the corresponding formamides at room temperature under solvent-free conditions. This method has the advantages of high yields, mild conditions, simple methodology, easy work up and short reaction times. … The Natrolite zeolite was recovered and reused several times without the significant loss of its catalytic performance" (Habibi et al., 2013).

The "green synthesis of a natrolite zeolite/palladium nanocomposite" was proposed in 2015, by Hatamifard et al., "and its application as a reusable catalyst for the reduction of organic dyes in a very short time". "A natrolite zeolite/palladium (natrolite zeolite/Pd) nanocomposite has been successfully synthesized applying a simple in situ reduction method using an aqueous extract of fruits of Piper longum as a reducing and stabilizing agent. … The catalytic activity of the natrolite zeolite/Pd nanocomposite is excellent for organic dye reduction at room temperature and remains the same for several cycles" (Hatamifard et al., 2015).

"α-Aminophosphonates are synthesized efficiently by one-pot reaction of aldehydes or ketones, amines, trialkyl phosphites in the presence of Natrolite zeolite as a natural catalyst under solvent-free conditions. Furthermore, the catalyst can be reused several times without any significant loss of catalytic activity" (Bahari & Sajadi, 2017).

Reviews about zeolites and catalysis are given by Sun et al., 2021, Xu and Wu, 2022, Liang et al., 2021, Zhang et al., 2022.

Raman OH-stretching region

Here we consider the Raman broad scans on minerals of the natrolite group, scans which are published in the RRUFF database. Of the Raman broad scans, we will consider the range between 2000 and 4000 cm^{-1}, which contains the hydroxyls OH-stretching region. We have already considered this region when we studied the Raman spectroscopy of water; we proposed specifically the decomposition of this large OH-stretching band in components with the q-Gaussian profile (see Appendix). Being the q-parameter of q-Gaussian functions related to the correlation time of stochastic Kubo modelling of fluctuations, we stressed the use of this parameter to characterize the local environments of O-H bonds. We further discussed the OH-stretching band of ice, to understand how the decomposition in q-Gaussians changes in the number of components and values of q-parameters. We have also considered the behavior of the Raman OH-stretching band in the case of the vivianite group of minerals. Here, we will apply the same approach, that is a decomposition of the spectrum in q-Gaussian components, to the scans on zeolites of the natrolite group.

Literature about the natrolite and its Raman spectroscopy is as follow.

Pechar and Rykl, 1983, proposed a study of the vibrational spectra of natrolite. "Three principal optical methods can be used to measure the vibrational spectra of crystals: l) the absorption of infrared radiation, 2) the reflectance of infrared radiation, and 3) the Raman scattering of visible radiation. … Infrared absorption spectra in the far-infrared and infrared region are suitable especially for the determination of vibrations of water molecules, hydroxyl groups and local bonds in the structure of minerals. … The Raman and reflection spectra of polycrystalline natrolite have not been published yet [in 1983 and according to Pechar and Rykl' knowledge]" (Pechar & Rykl, 1983). "Bands of the antisymmetrical and symmetrical vibration of hydroxyl groups lie in the region 3300-3610 cm^{-1}. They have a very strong intensity in the IR spectra and a low intensity in the Raman spectra. The shift of this vibration relative to the wavenumber of the same vibration for water vapor indicates the presence of hydrogen bonds" (Pechar and Rykl, mentioning Hamilton and Ibers 1968).

In the Table II of the article by Pechar and Rykl, we have data, here proposed in our Table I.

Table I (Vibrational spectra, cm^{-1})

Type of vibration	IR absorption	Raman	Theoretical freq.
OH stretching	3310-3515 Very strong	3300-3610 Weak	3656
H_2O bending	1625 Medium	1610 Very weak	1653

Goryainov and Smirnov, 2001, proposed "Raman spectra and lattice-dynamical calculations of natrolite". "Polarized single-crystal Raman scattering and powder infrared absorption spectra of Fdd2 orthorhombic natural natrolite" were measured. The lattice-dynamical calculations were made for the ideal natrolite structure. "The strongest Raman band at 534 cm^{-1} corresponds to a breathing mode of the four-membered aluminosilicate ring".

In the Table 1 of Goryainov and Smirnov, we find the following centers of peaks (cm^{-1}).

3189, 3225, 3331, 3384, 3475, 3543

3186, 3227, 3331, 3386, 3473

3187, 3226, 3331, 3384, 3473, 3542

3190, 3227, 3330, 3385, 3472, 3542

3183, 3228, 3330, 3386, 3472, 3542

3183, 3227, 3329, 3385, 3471, 3541

3184, 3229, 3328, 3385, 3472, 3543

"There is a remarkable agreement between the polarization of Raman spectra involving O-H (O-D) stretching vibrations and the calculated intensity. Fig. 1 [in Goryainov and Smirnov, 2001] shows that in the (*a,b*)-plane the 3542-cm^{-1} band is almost completely (*aa*)-polarized along the *a*-axis, whereas the 3331-cm^{-1} band is almost completely (*bb*)-polarized along the *b*-axis. This polarization is explained by orientation of the bonds and localization of stretching vibrations in one of two O-H bonds with corresponding alternative amplitudes of H2 or H1 atoms, …, due to strongly different force constants. Viewing natrolite in the (*a,b*) plane shows that O-H1 bond is nearly parallel to the *b*-axis, whereas O-H2 bond is nearly parallel to the *a*-axis" (Goryainov & Smirnov, 2001).

"The Raman spectrum of water in natural natrolite in Fig. 1 exhibits two main O-H bands at $\nu_1 = 3331$ cm^{-1} and $\nu_3 = 3542$ cm^{-1} and several additional bands of smaller intensity, which can be combined in two doublets at $\nu'_1 = 3187$, $\nu'_3 = 3385$ and $\nu''_1 = 3226$, $\nu''_3 = 3473$ cm^{-1}. These two doublets can be ascribed to vibration of H_2O molecules located in two additional sites in the crystal, W' and W'', with approximate relative occupancy of about 5% with respect to that of the main W site, which is almost completely occupied. This assumption is supported by the chemical composition of natural natrolite, which shows an excess of water of at least 1.5 % (or 0.03 H_2O per ideal 2 H_2O formula unit)" (Goryainov & Smirnov, 2001).

Kolesov and Geiger, 2006, studied the "behavior of H_2O molecules in the channels of natrolite and scolecite", by means of single-crystal polarized Raman spectra and IR spectroscopy. "Both IR and Raman spectra show intense O-H stretching and H_2O bending modes derived from the hydrogen-bonded H_2O molecule(s) in the channels. Using published crystal structural data for natrolite and scolecite, and a consideration of Raman mode intensities that are sensitive to the H_2O orientation in the framework channels, the internal stretching and bending modes could be assigned" (Kolesov & Geiger, 2006). "The stretching vibrations of H_2O molecules of natrolite and scolecite are located between 3200 and 3700 cm^{-1} and bending vibrations occur around 1650 cm^{-1}. In the case of natrolite, two intense O-H stretching modes can be observed and also several weaker combination modes. … For scolecite, six O-H stretching modes are observed in the Raman spectra recorded at 4 K, but only five are found at room temperature in the IR or Raman" (Kolesov & Geiger, 2006). In Kolesov and Geiger we can find crystal structures, with occluded H_2O of natrolite and scolecite. In natrolite, the H_2O molecules and Na cations are placed in the channel cavities. Na cations are in the center of the channel, whereas the H_2O molecules are located closer the walls of the channel. In the Fig,1(b) by Koleson and Geiger, we can see each H_2O molecule, with the Ow atom bonded to two Na atoms, and the two hydrogen atoms, H1 and H2, bonded to two different O atoms of the framework (Kolesov & Geiger, 2006).

Scolecite has a reduced symmetry, related to the difference in the channel content. In this mineral, we find "only one Ca and three H_2O molecules". "Indeed, one Na site in natrolite is replaced by one H_2O molecule … The Ca cation is bonded to four O atoms of the framework and three O atoms of H_2O molecules. All three H_2O molecules are characterized by slightly different O···H bond lengths and thus have slightly different O-H bond strengths" (Kolesov and Geiger, mentioning Kvick & Ståhl, 1985). The Figures 3a and 3b by Kolesov and Geiger are showing the polarized Raman spectra of natrolite at 4 K and room temperature, in the regions of H_2O stretching and bending vibrations. "The spectra at 298 K show two main bands at 3324 and 3538 cm^{-1} and several others of weaker intensity". The polarized Raman spectroscopy of scolecite shows that the "band at 3503 cm^{-1} at room temperature appears to split into two bands at 3493 and 3498 cm^{-1} in the 4 K spectra".

For what is regarding natrolite, "Two intense O-H stretching modes are observed in the IR and Raman spectra of natrolite. The low-wavenumber mode at ~3320 cm^{-1} represents to a large degree the motion of the more strongly H-bonded hydrogen atom of the H_2O molecule. The high-wavenumber band at ~3540 cm^{-1} is related to an O-H mode related to the moreweakly H-bonded hydrogen atom. The former mode derives from the ν_1 mode of a free symmetric H_2O molecule and the latter from the asymmetric vibration, ν_3" (Kolesov & Geiger, 2006). "The band at 3469 cm^{-1} in the Raman *bb*-spectrum at room temperature … is separated from the intense Ow-H1 stretching band at ~3320 (3324 cm^{-1} at room temperature) by 146 cm^{-1}. The band at 3179 cm^{-1} … appears in both Raman and IR spectra at temperatures greater than 80 K … and is separated from the band at 3320 cm^{-1} by approximately the same value, 144 cm^{-1}, but is located at lower energies. Thus, [Kolesov and Geiger] interpret these two weak Raman bands as Stokes (3469 cm^{-1}) and anti-Stokes (3179 cm^{-1}) counterparts of the same combination mode … . Note that the band at 3469 cm^{-1} is not a single combination mode. A deconvolution into *Lorentzian components* produces weak features at approximately 3369, 3392, 3426, and 3495 cm^{-1} … in the unpolarized Raman and IR spectra" (See the further discussion in Kolesov and Geiger, 2006). Therefore, we have bands given at: 3179, 3324, 3369, 3391, 3426, 3495 cm^{-1}.

RRUFF database - The aim of the RRUFF Project is that of creating "a complete set of high-quality spectral data from well characterized minerals". Moreover, RRUFF "is developing the technology to share this information with the world". Further information about the project is given in Lafuente et al., 2015. In RRUFF we can find several spectra of natrolite. To decompose them, we will use the q-Gaussian functions (see Appendix).

Name: Natrolite. RRUFF ID: R040022. Locality: Patterson, Passaic County, New Jersey, USA. Source: University of Arizona Mineral Museum 2108. Owner: RRUFF. Description: White fine fibrous mass. Status: The identification of this mineral has been confirmed by X-ray diffraction and chemical analysis. Unoriented sample. Instrument settings: Thermo Almega XR 532nm @ 100% of 150mW. Data as given by the link, used in the range from 3000 to 4000 cm^{-1}. A spline baseline adjustment is applied.

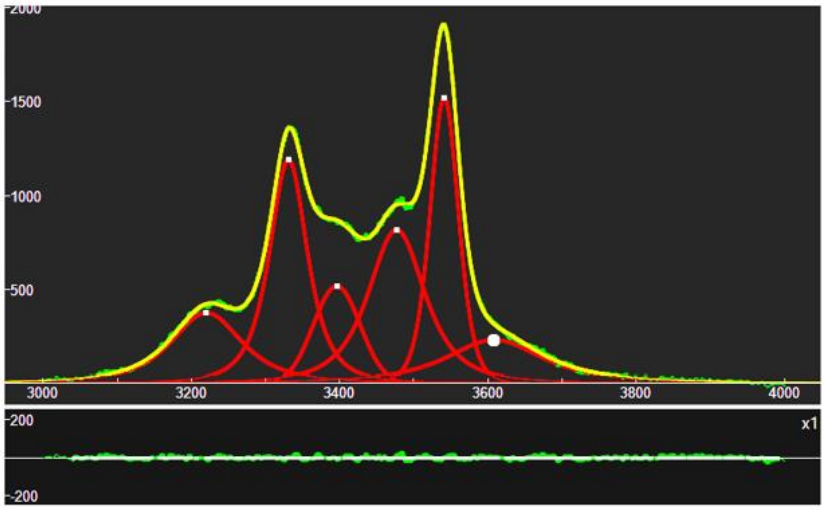

Fig.1: Deconvolution of natrolite RRUFF R040022 spectrum. The OH-stretching region is decomposed into six q-Gaussian bands (red curves). The centers of the components are at 3220, 3331, 3396, 3477, 3541, 3609 cm^{-1}.The lower part of the image is showing the misfit, that is the difference between data (green) and the sum of components (yellow curve).

The plot in the Fig.1, as in all figures, is obtained by means of software Fityk (Wojdyr, 2010), after defining in it the q-Gaussian functions (see Appendix for further details).

Natrolite RRUFF ID: R040102. Locality: Ross' Quarry, Northland, New Zealand. Source: University of Arizona Mineral Museum 12862. Owner: RRUFF. Description: Mass of colorless acicular crystals. The identification of this mineral has been confirmed by X-ray diffraction and chemical analysis. Unoriented sample. Instrument settings: Thermo Almega XR 532nm @ 100% of 150mW. Data as given by the link, used in the range from 3000 to 4000 cm^{-1}. A spline baseline adjustment is applied.

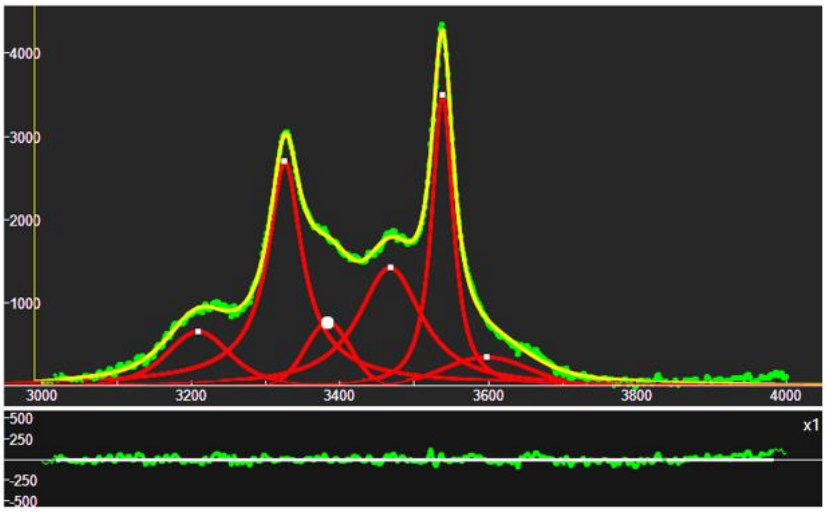

Fig.2: Deconvolution of natrolite RRUFF R040102 spectrum. As in the previous figure, the OH-stretching region is decomposed into six q-Gaussian bands. The centers of the components are at 3209, 3326, 3384, 3467, 3538, 3597 cm^{-1}.

Natrolite RRUFF ID: R040112. Locality: Ice River Alkaline Complex, Moose Creek Valley, Yoho National Park, British Columbia, Canada. Source: National Museums of Canada 061565. Owner: RRUFF. Description: Colorless pseudohexagonal prism. The identification of this mineral has been confirmed by X-ray diffraction and chemical analysis. Unoriented sample. Instrument settings: Thermo Almega XR 532nm @ 100% of 150mW. Data as given by the link, used in the range from 3000 to 4000 cm^{-1}. A spline baseline adjustment is applied.

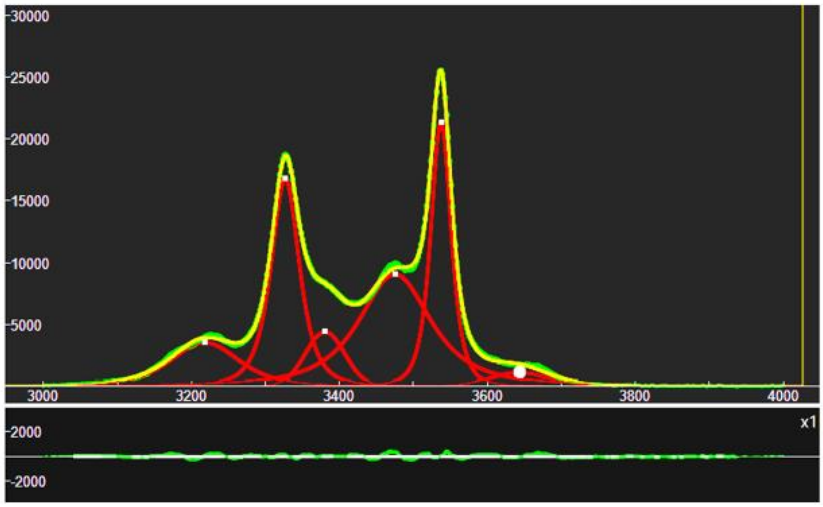

Fig.3: Deconvolution of natrolite RRUFF R040112 spectrum. As in the previous figure, the OH-stretching region is decomposed into six q-Gaussian bands. The centers of the six components are at 3218, 3327, 3380, 3475, 3537, 3643 cm^{-1}.

Natrolite RRUFF ID: R050589. Locality: Mont Saint-Hilaire, Rouville County, Quebec, Canada. Source: Bob Downs. Owner: RRUFF. Description: White to colorless prismatic crystals associated with aegirine. The identification of this mineral has been confirmed by X-ray diffraction and chemical analysis. Unoriented sample. Instrument settings: Thermo Almega XR 532nm @ 100% of 150mW.

Data as given by the link, used in the range from 3000 to 4000 cm^{-1}. A spline baseline adjustment is applied.

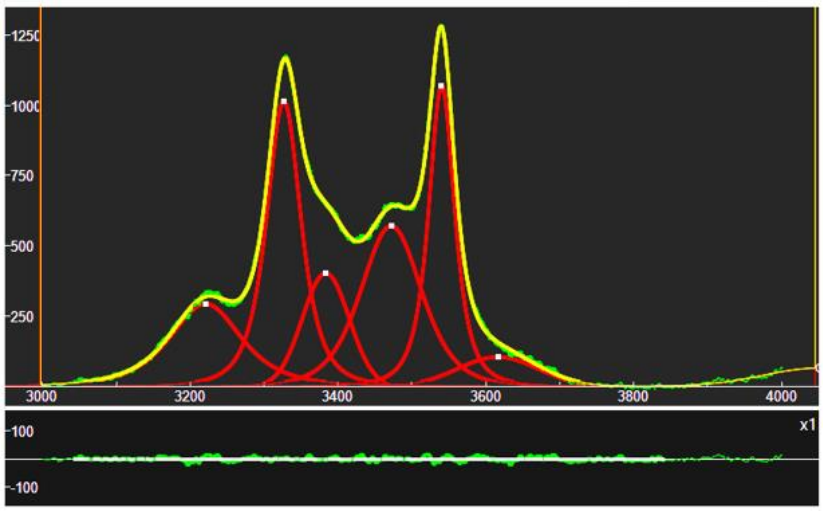

Fig.4: Deconvolution of natrolite RRUFF R050589 spectrum. As in the previous figure, the OH-stretching region is decomposed into six q-Gaussian bands. The centers of the six components are at 3221, 3327, 3383, 3472, 3540, 3616 cm^{-1}.

Natrolite RRUFF ID: R060561. Locality: California, USA. Source: Gemological Institute of America 13. Owner: RRUFF. Description: White fragment. The identification of this mineral has been confirmed by X-ray diffraction and chemical analysis. Unoriented Raman on the primary sample. Instrument settings: Thermo Almega XR 532nm @ 100% of 150mW. Data as given by the link, used in the range from 3000 to 4000 cm^{-1}. A spline baseline adjustment is applied.

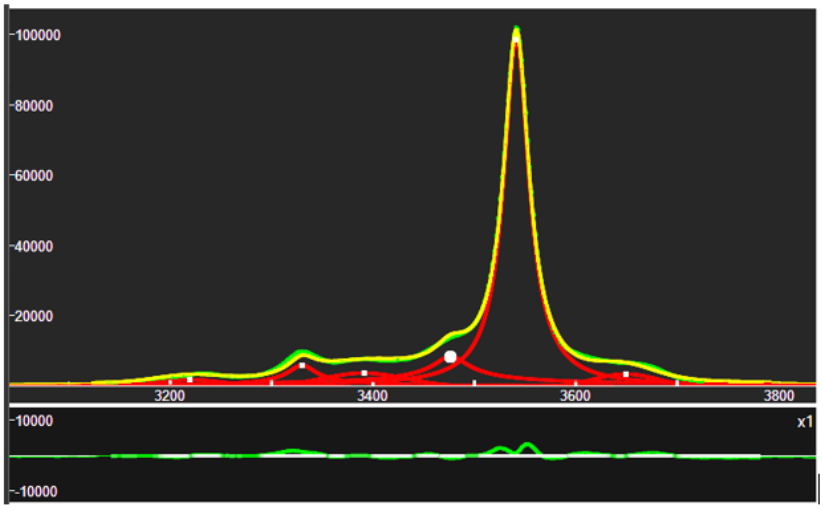

Fig.5: Deconvolution of natrolite RRUFF R060561 spectrum. As in the previous figure, the OH-stretching region is decomposed into six q-Gaussian bands. The centers of the six components are at 3220, 3330, 3391, 3477, 3541, 3649 cm^{-1}.

Another natrolite spectrum (RRUFF ID: R120124) is given in the database. However, it is not possible to investigate the OH-stretching region.

In the following table, the centers of the components are proposed.

R040022 spectrum. 3220, 3331, 3396, 3477, 3541, 3609 cm^{-1}

R040102 spectrum. 3209, 3326, 3384, 3467, 3538, 3597 cm^{-1}

R040112 spectrum. 3218, 3327, 3380, 3475, 3537, 3643 cm^{-1}

R050589 spectrum. 3221, 3327, 3383, 3472, 3540, 3616 cm^{-1}

R060561 spectrum. 3220, 3330, 3391, 3477, 3541, 3649 cm^{-1}

We can compare with literature (let us consider Figs. 3b,4b in Kolesov and Geiger).

Goryainov & Smirnov, 2001. 3187, 3226, 3331, 3385, 3473, 3542 cm^{-1}

Kolesov & Geiger, 2006. 3179, 3224, 3324, 3489, 3538 cm^{-1}

Kolesov & Geiger, 2006. 3179, 3324, 3538 cm^{-1}

For what is regarding the number of components, we used six q-Gaussians and obtained good fits. Of course, we could add further components, but it seems not being necessary. Another fact is to observe: the absence in literature of the band between 3600 and 3650 cm^{-1}. Let us pass to analyze the scolecite.

Scolecite RRUFF ID: R040111. Ideal Chemistry: $Ca(Si_3Al_2)O_{10}\cdot 3H_2O$. Locality: Bombay-Poona area, Mahahashtra Province, India. Source: National Museums of Canada 060318. Owner: RRUFF. Pale pink prismatic crystals in parallel or near parallel aggregates. The identification of this mineral has been confirmed by X-ray diffraction and chemical analysis. Unoriented sample. Instrument settings: Thermo Almega XR 532nm @ 100% of 150mW. Data as given by the link, used in the range from 3000 to 4000 cm^{-1}. A spline baseline adjustment is applied.

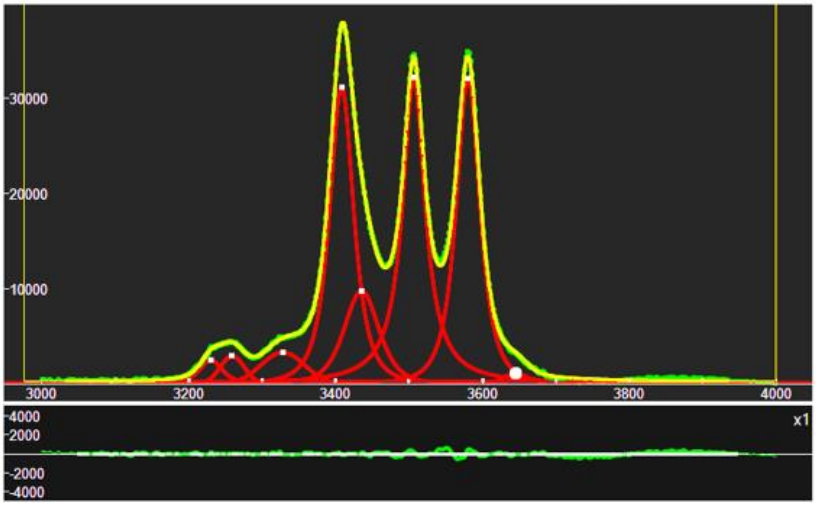

Fig.6: Deconvolution of scolecite RRUFF R040111 spectrum. The centers of the eight components are at 3230, 3259, 3328, 3408, 3435, 3506, 3580, 3645 cm^{-1}.

Scolecite RRUFF ID: R050083. Locality: near Ahmednagar, Maharashtra, India. Source: Rock Currier. Owner: RRUFF. Description: Colorless acicular single crystals associated with fluorapophyllite. Status: The identification of this mineral has been confirmed by X-ray diffraction and chemical analysis. Unoriented sample. Instrument settings: Thermo Almega XR 532nm @ 100% of 150mW. Data as given by the link, used in the range from 3000 to 4000 cm^{-1}. A spline baseline adjustment is applied.

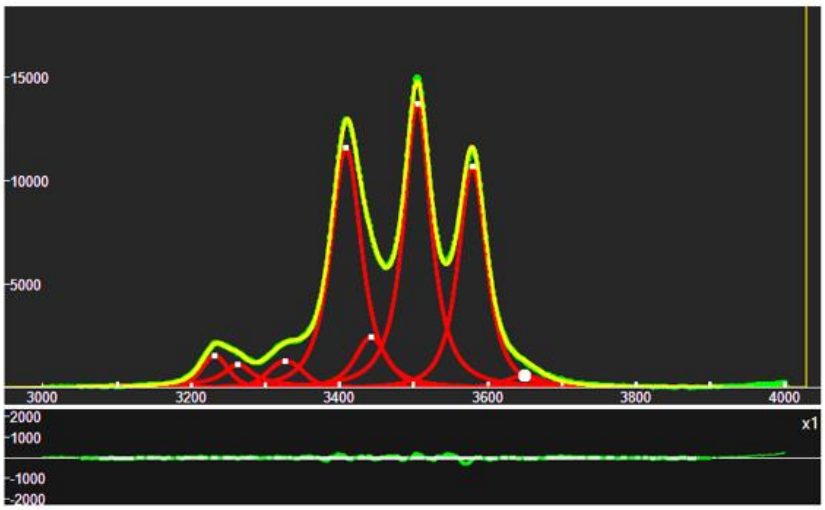

Fig.7: Deconvolution of scolecite RRUFF R050083 spectrum. The centers of the eight components are at 3232, 3263, 3327, 3409, 3442, 3505, 3579, 3650 cm^{-1}.

The peak at about 3405-3410 cm^{-1} has a shoulder. Kolesov and Geiger are proposing the following data for scolecite, then we can provide the following comparison.

Centers of components (in cm^{-1}).

R040111	3230	3259	3328	3408	3435	3506	3580	3645
R050083	3232	3264	3327	3409	3442	3505	3579	3650
Kolesov Geiger	3230		3325	3406		3503	3580	

Another member of the natrolite group is the mesolite. Its name is coming from the Greek mesos, "middle", because of its composition which lies between natrolite and scolecite.

Mesolite RRUFF ID: R050013, Ideal Chemistry: $Na_2Ca_2(Si_9Al_6)O_{30}·8H_2O$. Locality: Poona, Maharashtra, India. Source: University of Arizona Mineral Museum 10480. Owner: RRUFF. Description: Clear to white elongated prismatic single crystal. Status: The identification of this mineral has been confirmed by X-ray diffraction and chemical analysis. Unoriented sample. Instrument settings: Thermo Almega XR 532nm @ 100% of 150mW. Data as given by the link, used in the range from 3000 to 4000 cm^{-1}. A spline baseline adjustment is applied.

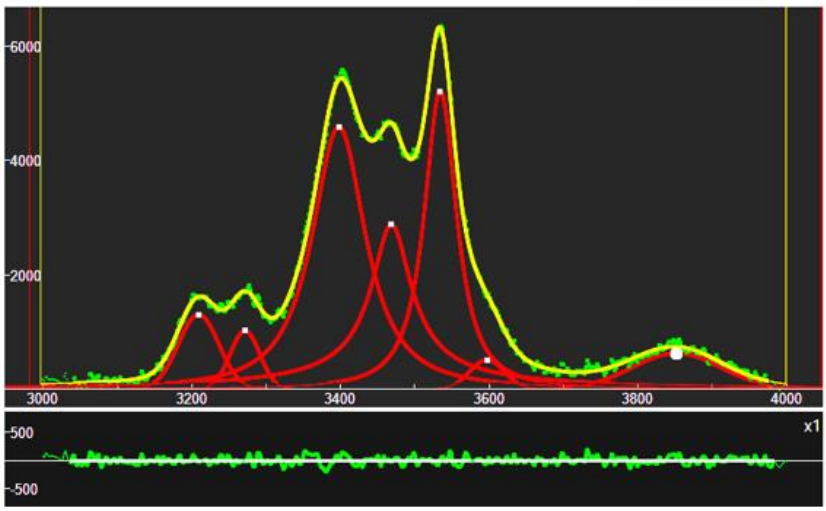

Fig.8: Deconvolution of mesolite RRUFF R050013 spectrum. The centers of the seven components are at 3209, 3271, 3398, 3468, 3534, 3597, 3852 cm^{-1}.

Mesolite RRUFF ID: R040139. Locality: Lake Superior beach, 41 miles north of Tofte, Minnesota, USA. Source: University of Arizona Mineral Museum 9618. Owner: RRUFF. Description: Aggregate f white radiating thin acicular crystals. Status: The identification of this mineral has been confirmed by X-ray diffraction and chemical analysis. Unoriented sample. Instrument settings: Thermo Almega XR 532nm @ 100% of 150mW. Data as given by the link, used in the range from 2500 to 4500 cm^{-1}. A spline baseline adjustment is applied.

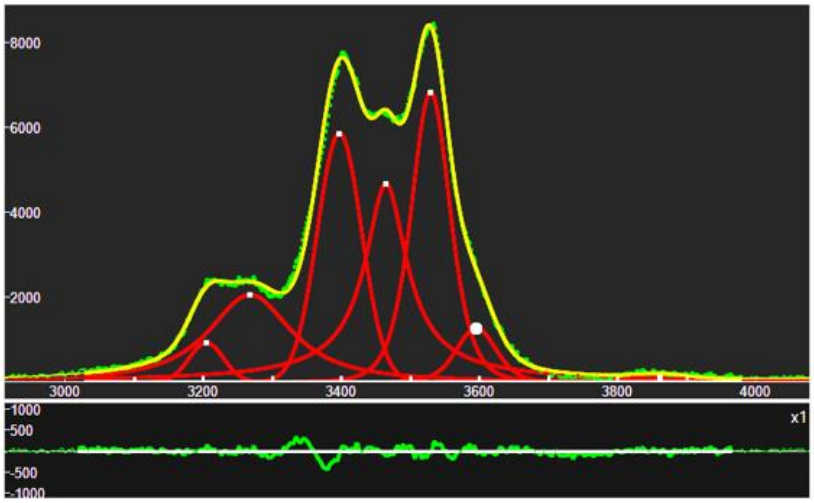

Fig.9: Deconvolution of mesolite RRUFF R040139 spectrum. The centers of the seven components are at 3204, 3268, 3397, 3465, 3529, 3595, 3861 cm^{-1}.

Mesolite RRUFF ID: R040140. Locality: Challis, Idaho, USA. Source: University of Arizona Mineral Museum 16169. Owner: RRUFF. Description: White fibrous mass, associated with barrierite. Status: The identification of this mineral has been confirmed by X-ray diffraction and chemical analysis. Unoriented sample. Instrument settings: Thermo Almega XR 532nm @ 100% of 150mW. Data as given by the link, used in the range from 2500 to 4000 cm^{-1}. A spline baseline adjustment is applied.

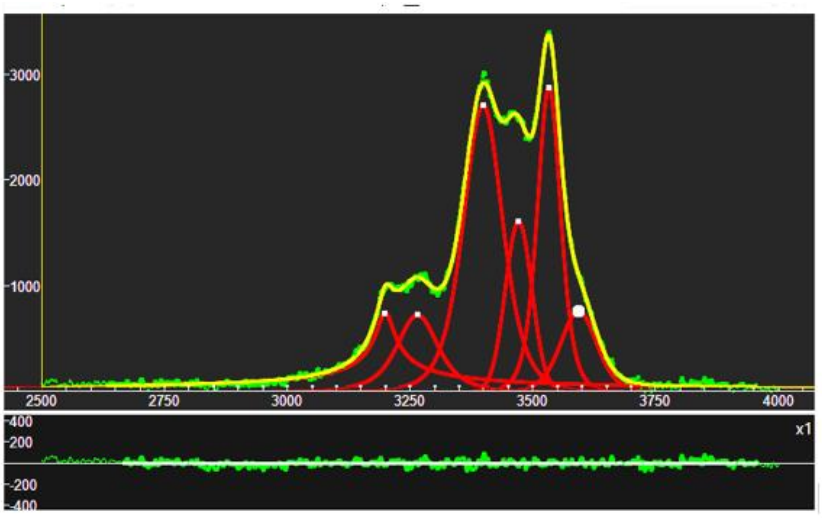

Fig.10: Deconvolution of mesolite RRUFF R040140 spectrum. The centers of the six components are at 3199, 3265, 3398, 3471, 3533, 3593 cm^{-1}.

The centers of the components (mesolite) are therefore:

R050013: 3209, 3271, 3398, 3468, 3534, 3597, 3852 cm^{-1}.

R040139: 3204, 3268, 3397, 3465, 3529, 3595, 3861 cm^{-1}.

R040140: 3199, 3265, 3398, 3471, 3533, 3593 cm^{-1}.

The last member of the group that we consider is the gonnardite.

Gonnardite RRUFF ID: R100080. Ideal Chemistry: $(Na,Ca)_2(Si,Al)_5O_{10}\cdot 3H_2O$. Locality: Rio Chiavone nero, Fara, Breganze, Vicenza, Italy. Source: Ivano Rocchetti. Instrument settings: Thermo Almega XR 532nm @ 100% of 150mW. Data as given by the link, used in the range from 2500 to 4500 cm^{-1}. A spline baseline adjustment is applied. Gonnardite RRUFF ID: R100081. Locality: Chaux de Bergonne, Gignat, Puy de Dome, France. Source: Ivano Rocchetti. Owner: RRUFF. Instrument settings: Thermo Almega XR 532nm @ 100% of 150mW. Data as given by the link, used in the range from 2500 to 4500 cm^{-1}. A spline baseline adjustment is applied.

In the following figures, we propose decompositions in three and four q-Gaussians.

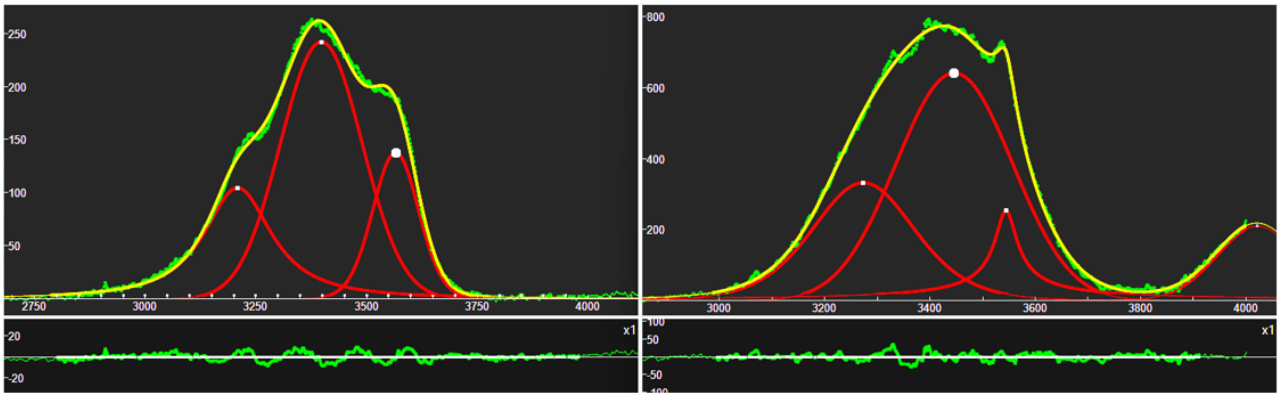

Fig.11. On the left, R100080, centers at 3209, 3398, 3566 cm^{-1}. On the right, R100081, centers at 3273, 3446, 3544 cm^{-1}.

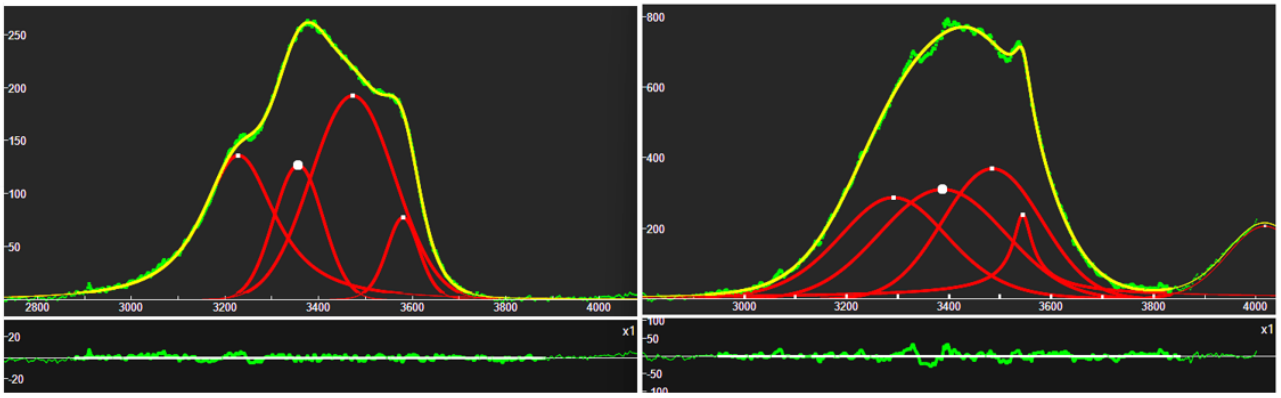

Fig.12. On the left, R100080, centers at 3229, 3357, 3472, 3580 cm^{-1}. On the right, R100081, centers at 3292, 3388, 3485, 3544 cm^{-1}.

In Tsai et al., 2021, we can find the natrolite group including thomsonite and edingtonite. Tsai and coworkers do not consider the OH-stretching region, but we can find the related bands discussed in a reference mentioned by the researchers. In Wopenka et al., 1998, we can find the following results (centers of the peaks in cm^{-1}).

Natrolite			3231	3329	3476	3543	
Mesolite	3080,3087	3182	3212	3405	3472	3536	
Scolecite			3242	3329	3412	3510	3583
Thomsonite			3289		3417		
Gonnardite			3231		3444		
Edingtonite					3480		

By Wopenka and coworkers, we find stressed that the natrolite group members have water inside, "and the specific positions of the H_2O molecules are controlled by the regular arrangement of the channels and cages that exist in a given crystal lattice". The peaks observed in the OH-stretching region "are among the most characteristic ones for a given natrolite group mineral and *can be used for unambiguous identification*. Natrolite, mesolite, and scolecite (all structural type 3) are characterized by several sharp peaks in this spectral region, and thomsonite and gonnardite (both structural type 2) have a broad unresolved double peak feature, whereas edingtonite (structural type 1) has a medium wide single peak. Among the six members of the group, mesolite has the weakest bands in the OH stretching region, followed by gonnardite. The other four natrolite group minerals are all characterized by strong bands in the OH spectral region. Scolecite, which has the most characteristic feature in the OH stretching region, is characterized by five narrow well-resolved peaks" (Wopenka et al., 1998).

In RRUFF database we can find spectra of thomsonite and edingtonite, so let us add q-Gaussian deconvolution of these spectra too.

Thomsonite-Ca RRUFF ID: R050091. Ideal Chemistry: $NaCa_2(Al_5Si_5)O_{20}\cdot 6H_2O$. Locality: Amudikha River, near Mirny, Yakutia, Siberia, Russia. Source: Rock Currier. Owner: RRUFF. Instrument settings: Thermo Almega XR 532nm @ 100% of 150mW. Data as given by the link, used in the range from 2500 to 4500 cm^{-1}. A spline baseline adjustment is applied. RRUFF ID: R050103. Locality: Seeberg, Bohemia, Czech Republic. Source: Rock Currier. Owner: RRUFF. Instrument settings: Thermo Almega XR 532nm @ 100% of 150mW. Data as given by the link, used in the range from 2500 to 4500 cm−1. A spline baseline adjustment is applied.

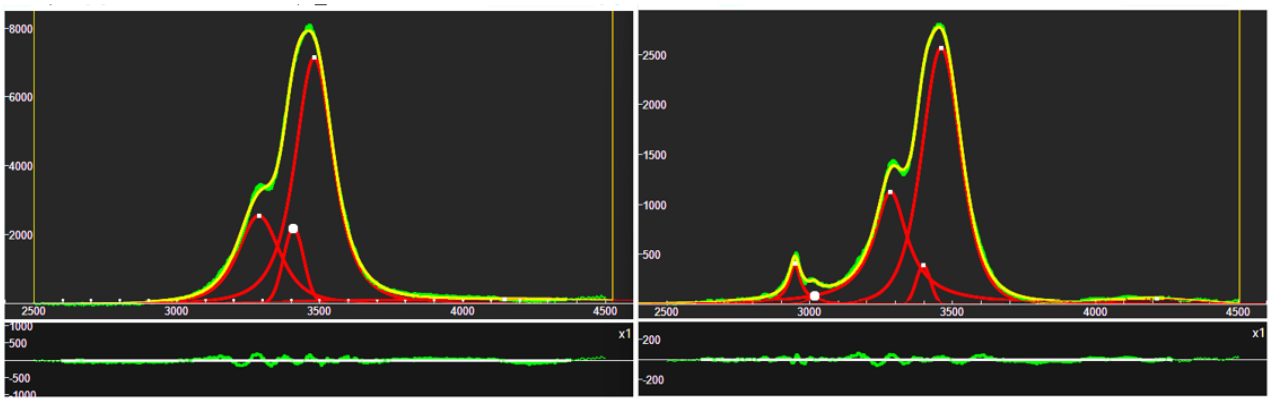

Fig.13. Thomsonite. On the left, R050091, centers at 3286, 3408, 3481 cm^{-1}. On the right, R050103, centers at 2948, 3016, 3283, 3397, 3460 cm^{-1}.

Edingtonite, ideal chemistry: $Ba(Si_3Al_2)O_{10}\cdot 4H_2O$. RRUFF ID R040003: Locality: Bohl, Sweden. Source: University of Arizona Mineral Museum 2960. Owner: RRUFF. Instrument settings: Thermo Almega XR 532nm @ 100% of 150mW. We use data as given by the link, in the range from 3000 to 4000 cm^{-1}. A spline baseline adjustment is applied. RRUFF ID R040110: Locality: 2350 level, Brunswick 12 mine, Bathhurst, New Brunswick, Canada. Source: National Museums of Canada 014899. Owner: RRUFF. Data as given by the link, used in the range from 3000 to 4000 cm^{-1}. A spline baseline adjustment is applied.

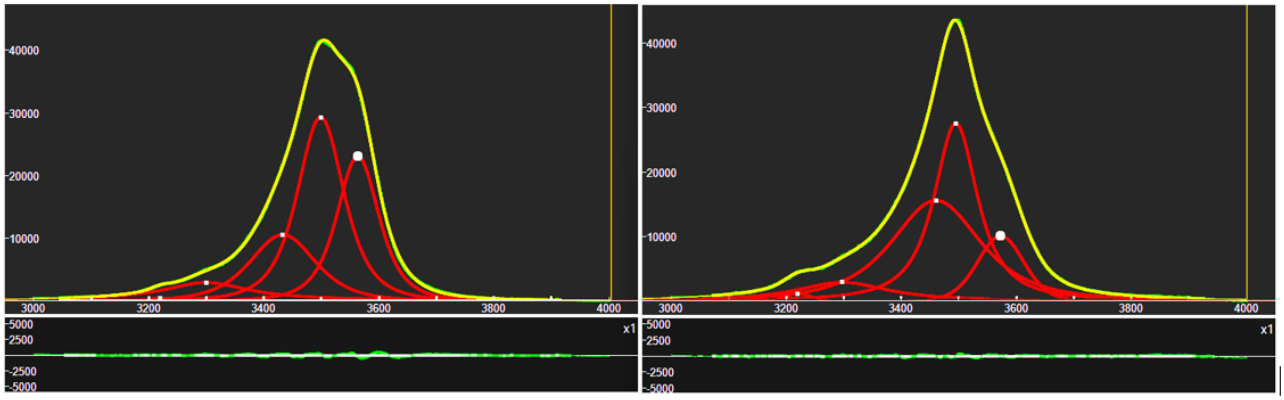

Fig.14. Edingtonite. On the left, R040003, centers at 3220, 3300, 3433, 3499, 3563 cm^{-1}. On the right, R040110, centers at 3219, 3297, 3460, 3495, 3573 cm^{-1}.

Here in the following, the centers of the components of gonnardite, thomsonite and edingtonite are given.

Gonnardite R100080, 3229, 3357, 3472, 3580 cm^{-1}.

Gonnardite R100081, 3292, 3388, 3485, 3544 cm^{-1}.

Thomsonite R050091, 3286, 3408, 3481 cm^{-1}.

Thomsonite R050103, 2948, 3016, 3283, 3397, 3460 cm^{-1}.

Edingtonite R040003, 3220, 3300, 3433, 3499, 3563 cm^{-1}.

Edingtonite R040110, 3219, 3297, 3460, 3495, 3573 cm^{-1}.

Conclusion

In our discussion, we have shown the OH-stretching region of Raman spectra, in the case of natrolite, scolecite, mesolite and gonnardite. The results of gonnardite have been compared to those of thomsonite and edingtonite. As stressed by Wopenka et al., 1998, the Raman spectroscopy is able of distinguishing the minerals, due to their water content too. What could be interesting for future research, is the investigation of the Raman spectra of materials with ion exchange and of super-hydrated minerals. Moreover, the synthetic zeolite A could be able of provide information about the water and its behavior in the framework.

Appendix – q-Gaussian functions

The q-Gaussian functions are probability distributions proper of the Tsallis statistics (Tsallis, 1988, Hanel et al., 2009). These functions are based on a generalized form of the exponential function, characterized by a continuous real parameter q. When q is going to 1, the q-exponential becomes the usual exponential function. The value q=2, (Naudts, 2009), corresponds to the Cauchy distribution, also known as the Lorentzian distribution; the q-Gaussian function is therefore a generalization of the Lorentzian distribution too. The change of q-parameter is allowing the q-Gaussian function to pass from the Gaussian to the Lorentzian distribution. Sparavigna, 2023, proposed for the first time the use of q-Gaussian function in Raman spectroscopy.

As given by Umarov et al., 2008, the q-Gaussian function is: $f(x) = Ce_q(-\beta x^2)$, where $e_q(.)$ is the q-exponential function and C a scale constant (in the exponent, $\beta = 1/(2\sigma^2)$). The q-exponential has expression: $e_q(u) = [1 + (1-q)u]^{1/(1-q)}$.

In Fityk software, a q-Gaussian function can be defined in the following manner:

define Qgau(height, center, hwhm, q=1.5) = height*(1+(q-1)*((x-center)/hwhm)^2)^(1/(1-q))

q=1.5 the initial guessed value of the q-parameter. Parameter hwhm is the half width at half maximum of the component. When q=2, the q-Gaussian is a Lorentzian function, that we can find defined in Fityk as:

Lorentzian(height, center, hwhm) = height/(1+((x-center)/hwhm)^2)

When q is close to 1, the q-Gaussian becomes a Gaussian function.

References

1. Ackley, M. W., Rege, S. U., & Saxena, H. (2003). Application of natural zeolites in the purification and separation of gases. Microporous and Mesoporous Materials, 61(1-3), 25-42.
2. Bahari, S., & Sajadi, S. M. (2017). Natrolite zeolite: A natural and reusable catalyst for one-pot synthesis of α-aminophosphonates under solvent-free conditions. Arabian Journal of Chemistry, 10, S700-S704.
3. Clifton, R. A. (1987). Natural and synthetic zeolites (Vol. 9140). US Department of the Interior, Bureau of Mines.
4. Dudka, A. P., Bedran, Z. V., Belyanchikov, M. A., & Gorshunov, B. P. (2020). Accurate Crystal Structure Refinement of Natrolite and Localization of Free Water. Crystallography Reports, 65, 862-870.
5. Dutta, P. K., & Del Barco, B. (1985). Raman spectroscopic studies of zeolite framework. Hydrated zeolite A and the influence of cations. The Journal of Physical Chemistry, 89(10), 1861-1865.
6. Dutta, P. K., & Del Barco, B. (1988). Raman spectroscopy of zeolite A: influence of silicon/aluminum ratio. The Journal of Physical Chemistry, 92(2), 354-357.
7. Dyar, M.D., Jawin, E.R., Breves, E., Marchand, G., Nelms, M., Lane, M.D., Mertzman, S.A., Bish, D.L., & Bishop, J.L. (2014). Mössbauer parameters of iron in phosphate

minerals: Implications for interpretation of martian data. American Mineralogist, 99(5-6), pp.914-942.
8. Dyer, A. (2000). Ion exchange. Encyclopedia of Separation Science, 156-173.
9. Dyer, A. (2005). Ion-exchange properties of zeolites. In Studies in Surface Science and Catalysis (Vol. 157, pp. 181-204). Elsevier.
10. Dyer, A. (2007). Ion-exchange properties of zeolites and related materials. In Studies in surface science and catalysis (Vol. 168, pp. 525-553). Elsevier.
11. Galitskii, V. Y., & Kozlov, A. M. (1988). Pyroelectric properties of natural natrolite Na/sub 2/Al/sub 2/Si/sub 3/O/sub 10//times/2H/sub 2/O. Inorg. Mater.(Engl. Transl.);(United States), 23(11).
12. Galitskii, V. Y., & Kozlov, A. M. (1987). Pyroelectric properties of natural natrolite Na2Al2Si3O10. 2H2O. Inorganic Materials, 23(11), 1698-1699.
13. Gorshunov, B.P., Torgashev, V.I., Zhukova, E.S., Thomas, V.G., Belyanchikov, M.A., Kadlec, C., Kadlec, F., Savinov, M., Ostapchuk, T., Petzelt, J., & Prokleška, J. (2016). Incipient ferroelectricity of water molecules confined to nano-channels of beryl. Nature communications, 7(1), p.12842.
14. Goryainov, S. V., & Smirnov, M. B. (2001). Raman spectra and lattice-dynamical calculations of natrolite. Eur. J. Mineral., 13, 507-519
15. Habibi, D., Nasrollahzadeh, M., & Sahebekhtiari, H. (2013). Green synthesis of formamides using the Natrolite zeolite as a natural, efficient and recyclable catalyst. Journal of Molecular Catalysis A: Chemical, 378, 148-155.
16. Halla, F., & Mehl, E. (1932). Zeits. Krist., vol. 83, p. 140.
17. Hamilton, W. C. (1968). Hydrogen bonding in solids. Methods of Molecular Structure Determination. Frontiers in Chemistry.
18. Hanel, R., Thurner, S., & Tsallis, C. (2009). Limit distributions of scale-invariant probabilistic models of correlated random variables with the q-Gaussian as an explicit example. The European Physical Journal B, 72(2), 263.
19. Hatamifard, A., Nasrollahzadeh, M., & Lipkowski, J. (2015). Green synthesis of a natrolite zeolite/palladium nanocomposite and its application as a reusable catalyst for the reduction of organic dyes in a very short time. RSC advances, 5(111), 91372-91381.
20. Hey, M. H. (1932). Studies on the zeolites. Part III. Natrolite and metanatrolite. Mineralogical magazine and journal of the Mineralogical Society, 23(139), 243-289.
21. Hill, G. L., Bailey, E., Stennett, M. C., Hyatt, N. C., Maddrell, E. M., McMillan, P. F., & Hriljac, J. A. (2011). High-pressure and-temperature ion exchange of aluminosilicate and gallosilicate natrolite. Journal of the American Chemical Society, 133(35), 13883-13885.
22. Julbe, A., & Drobek, M. (2016). Zeolite A Type. In: Drioli, E., Giorno, L. (eds) Encyclopedia of Membranes. Springer, Berlin, Heidelberg. https://doi.org/10.1007/978-3-662-44324-8_604
23. Kolesov, B. A., & Geiger, C. A. (2006). Behavior of H2O molecules in the channels of natrolite and scolecite: A Raman and IR spectroscopic investigation of hydrous microporous silicates. American Mineralogist, 91(7), 1039-1048.
24. Kvick, Å., & Ståhl, K. (1985). A neutron diffraction study of the bonding of zeolitic water in scolecite at 20 K. Zeitschrift für Kristallographie-Crystalline Materials, 171(1-4), 141-154.
25. Lafuente, B., Downs, R. T., Yang, H., & Stone, N. (2015). 1. The power of databases: The RRUFF project. In Highlights in mineralogical crystallography (pp. 1-30). De Gruyter (O).
26. Lee, Y., Lee, Y., & Seoung, D. (2010). Natrolite may not be a “soda-stone” anymore: Structural study of fully K-, Rb-, and Cs-exchanged natrolite. American Mineralogist, 95(11-12), 1636-1641.

27. Lee, Y., Liu, D., Seoung, D., Liu, Z., Kao, C. C., & Vogt, T. (2011). Pressure-and heat-induced insertion of CO2 into an auxetic small-pore zeolite. Journal of the American chemical society, 133(6), 1674-1677.
28. Liang, J., Shan, G., & Sun, Y. (2021). Catalytic fast pyrolysis of lignocellulosic biomass: Critical role of zeolite catalysts. Renewable and Sustainable Energy Reviews, 139, 110707.
29. Line, C. M., & Kearley, G. J. (1998). The librational and vibrational spectra of water in natrolite, Na2Al2Si3O10· 2H2O compared with ab-initio calculations. Chemical physics, 234(1-3), 207-222.
30. Meier, W. M. (1960). The crystal structure of natrolite. Zeitschrift für Kristallographie-Crystalline Materials, 113(1-6), 430-444.
31. Naudts, J. (2009). The q-exponential family in statistical physics. Central European Journal of Physics, 7, 405-413.
32. Paczwa, M., Sapiga, A. A., Olszewski, M., Sergeev, N. A., & Sapiga, A. V. (2016). Proton Dipolar Spin–Lattice Relaxation in Nano-channels of Natrolite. Applied Magnetic Resonance, 47, 895-902.
33. Pechar, F., & Rykl, D. (1983). Study of the vibrational spectra of natural natrolite. Canadian Mineralogist, 21(6), 89-695.
34. Sardashti, A. R., Kazemian, H., & Ardakani, M. A. (2001). 01-P-08-Chemical composition and ion-exchange properties of a natrolite from Zahedan region, Iran. Studies in Surface Science and Catalysis, 135, 240.
35. Sarkar, S., Ghosh, S., Mukherjee, A., Bose, N., & Ray, D. (2024). Detection of Natrolite on Mars Using Perseverance Rover Data. LPI Contributions, 3040, 1053.
36. Seryotkin, Y. V., Bakakin, V. V., Fursenko, B. A., Belitsky, I. A., Joswig, W., & Radaelli, P. G. (2005). Structural evolution of natrolite during over-hydration: a high-pressure neutron diffraction study. European journal of mineralogy, 17(2), 305-313.
37. Sparavigna, A. C. (2023). q-Gaussian Tsallis Line Shapes and Raman Spectral Bands. Int. J. Sciences, 12(3), 27-40.
38. Sparavigna, A. C. (2023). q-Gaussian Tsallis Line Shapes for Raman Spectroscopy (June 7, 2023). SSRN Electronic Journal. http://dx.doi.org/10.2139/ssrn.4445044
39. Sparavigna A. C. (2023). Tsallis q-Gaussian function as fitting lineshape for Graphite Raman bands. ChemRxiv. Cambridge: Cambridge Open Engage; 2023.
40. Sparavigna, A. C. (2023). SERS Spectral Bands of L-Cysteine, Cysteamine and Homocysteine Fitted by Tsallis q-Gaussian Functions. International Journal of Sciences, 12(09), 14–24. https://doi.org/10.18483/ijsci.2721
41. Sparavigna, A. C. (2024). Kubo Lineshape and its Fitted q-Gaussian Tsallis Function. International Journal of Sciences, 13(01), 1-9.
42. Sparavigna, A. C. (2024). Water, q-Gaussians and Raman Spectroscopy. International Journal of Sciences, 13(03), 17-25. http://dx.doi.org/10.18483/ijSci.2751
43. Sparavigna, A. C. (2024). Applying q-Gaussians to the OH-stretching Raman bands of Water and Ice. International Journal of Sciences, 13(04), 1-10. http://dx.doi.org/10.18483/ijSci.2756
44. Sparavigna, A. C. (2024). Hydroxyl-Stretching Region in the Raman Broad Scans on Minerals of the Vivianite Group (Vivianite, Baricite, Bobierrite, Annabergite, Erythrite). International Journal of Sciences, 13(08), 23–36. https://doi.org/10.18483/ijsci.2787
45. Strekeisen, A. (2020). Natrolite. https://www.alexstrekeisen.it/english/pluto/natrolite.php
46. Sun, Q., Wang, N., & Yu, J. (2021). Advances in catalytic applications of zeolite-supported metal catalysts. Advanced Materials, 33(51), 2104442.

47. Tsai, Y.L., Huang, E., Li, Y.H., Hung, H.T., Jiang, J.H., Liu, T.C., Fang, J.N., & Chen, H.F. (2021). Raman spectroscopic characteristics of zeolite group minerals. Minerals, 11(2), p.167.
48. Tsallis, C. (1988). Possible generalization of Boltzmann-Gibbs statistics. Journal of statistical physics, 52, 479-487.
49. Umarov, S., Tsallis, C., Steinberg, S. (2008). On a q-Central Limit Theorem Consistent with Nonextensive Statistical Mechanics. Milan J. Math. Birkhauser Verlag. 76: 307–328. doi:10.1007/s00032-008-0087-y. S2CID 55967725.
50. Wojdyr, M. (2010). Fityk: a general-purpose peak fitting program. Journal of applied crystallography, 43(5), 1126-1128.
51. Wopenka, B., Freeman, J. J., & Nikischer, T. (1998). Raman spectroscopic identification of fibrous natural zeolites. Applied Spectroscopy, 52(1), 54-63.
52. Xu, H., & Wu, P. (2022). New progress in zeolite synthesis and catalysis. National science review, 9(9), nwac045.
53. Zhang, Q., Gao, S., & Yu, J. (2022). Metal sites in zeolites: synthesis, characterization, and catalysis. Chemical reviews, 123(9), 6039-6106.